

## Magnetization behavior of nanometer-scale iron particles

S. Wirth

*MARTECH, Florida State University, Tallahassee, Florida 32306-4351*

M. Field and D. D. Awschalom

*Department of Physics, University of California, Santa Barbara, California 93106*

S. von Molnár

*MARTECH, Florida State University, Tallahassee, Florida 32306-4351*

(Received 23 December 1997)

The magnetic properties (magnetic moment, shape anisotropy, switching field, and distribution) of nanometer-scale ferromagnetic iron particles are investigated by measuring magnetization curves for different particle orientations. The measured switching fields indicate that magnetization curling accounts for the reversal at “zero” temperatures and an exchange length,  $\lambda_{ex}=2.6$  nm, is deduced. A phenomenological model describing the temperature dependence of the switching field is used to estimate the activation volume,  $v_A=270$  nm<sup>3</sup>. This is small compared to the particle volume and may explain the experimental fact that the magnetization reversal cannot be described by thermal activation over an average single energy barrier. [S0163-1829(98)51022-3]

The investigation of microscopic ferromagnetic particles is important for testing basic concepts of ferromagnetism<sup>1,2</sup> as well as gaining insight into the magnetic behavior of more complex structures (e.g., hard magnets). To this end, the development of micromagnet manufacturing techniques has been accompanied by sophisticated measurement techniques, e.g., near field magnetic force and Lorentz microscopy, micro superconducting quantum interference device and Hall magnetometry, and electron holography.

Here, we report on the switching behavior of arrays of nanometer-scale iron particles of approximately cylindrical shape. The ferromagnetic particles show shape anisotropy with an easy magnetization direction (EMD) parallel to the long axis. Magnetization curves are measured parallel and perpendicular to the EMD using an integrated Hall magnetometer whose response is calculated from the stray field of the dots. By fitting calculated magnetization curves to the measured hysteresis loops, we obtain information on the magnetization dynamics of the particles.

A combination of chemical vapor deposition (CVD) and scanning tunneling microscopy (STM) has been used<sup>3-5</sup> to fabricate the arrays of ferromagnetic iron particles. The number, location, and height of the particles in an array is controlled by steering the tip in a programmed array pattern. The particle array is grown directly onto a semiconductor Hall cross which is used as a compensation magnetometer.<sup>4</sup> The Hall voltage induced by the magnetic flux of the particles through the cross is detected to measure magnetization curves of the arrays.

The arrays are examined by scanning electron (SEM), atomic (AFM), and magnetic force (MFM) microscopy (cf. Ref. 6). Typical AFM (top) and MFM (bottom) images of identical parts of an array are presented in Fig. 1. From AFM measurements, the interparticle distance is  $\sim 300$  nm and the height is 170 nm. Earlier TEM studies<sup>3</sup> revealed that not all of the volume of each particle is magnetic but in fact, they

consist of a bcc iron core surrounded by a carbon coating which may come from the Fe(CO)<sub>5</sub> precursor. This coating is important for the stability of the particles as it reduces their oxidation and aging in air.

Magnetization curves of the particle arrays are measured from 10–100 K and with fields applied parallel and perpendicular to the particles' EMD. Also, MFM measurements which directly image the particle switching at a given field are performed at room temperature.

The response of the Hall magnetometer is induced by the particle magnetic stray field of the array which must be summed over the full active area of the Hall magnetometer. Since the dimensions of the array are of the same order of magnitude as the magnetometer dimensions, the field profile of the extended cylinders is calculated exactly rather than using a point-dipole approximation.

The particles' iron cores are assumed to be cylindrically shaped (height  $h$  and radius  $R$ , where  $R$  is determined experimentally from the stray field) and to have their magnetic

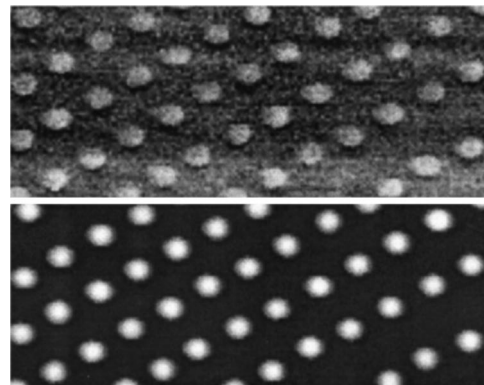


FIG. 1. AFM (top) and MFM (bottom) of identical portions (width 3  $\mu\text{m}$ ) of an array consisting of  $29 \times 21$  particles.

moments homogeneously distributed within their volume. For fields applied parallel to the particles' EMD, switching of the magnetization can be observed but reversal involves inhomogeneous magnetization modes even for particles as small as those discussed here.<sup>7-9</sup> In contrast, the reversible magnetization rotation<sup>10</sup> can be assumed to be homogeneous over the particle volume<sup>11</sup> and the exchange energy contribution to the particles' free energy density  $f$  vanishes. Reversible rotation is best observed for fields applied perpendicular to the EMD. Taking into account the Zeeman and anisotropy energy density results in

$$f = K_S \sin^2 \vartheta - J_S H \cos(\vartheta_H - \vartheta), \quad (1)$$

where  $\vartheta_H$  and  $\vartheta$  are the orientations of the applied field  $H$  and the particles' magnetization  $J_S$  with respect to the EMD, respectively. The shape anisotropy constant

$$K_S = (N_{\perp} - N_{\parallel}) J_S^2 / 2 \mu_0 \quad (2)$$

is related to the demagnetization factors parallel ( $N_{\parallel}$ ) and perpendicular ( $N_{\perp}$ ) to the particles' cylinder axis (i.e., the EMD). Magnetocrystalline anisotropy can be neglected since it is one order of magnitude smaller ( $K_1 = 53 \text{ kJm}^{-3}$ , Ref. 12) than shape anisotropy. The equilibrium orientation of the particles' magnetization  $\vartheta(H, \vartheta_H)$  can be determined by minimizing  $f$  with respect to  $\vartheta$ .

The magnetic stray field for an iron particle of known volume and (homogeneous) magnetization orientation can be calculated at any point of the active area of the Hall magnetometer by integration over magnetic surface charges. Here, only the  $z$  component of the stray field,  $H_z$ , normal to the plane of the Hall magnetometer (i.e., normal to the substrate surface) is relevant. The contributions of the two axial planes,  $H_z^a$ , and the radial plane,  $H_z^r$ , to the total stray field of the cylindrically shaped particles are considered separately

$$H_z = -H_z^a(h_i = z_d + h) + H_z^a(h_i = z_d) + H_z^r, \quad (3)$$

where  $h_i$  is the distance in the  $z$  direction between the axial plane under consideration (top or bottom of the cylindrical particle) and the active Hall layer and  $z_d$  is the thickness of the layer below which the active layer is buried underneath the substrate surface. In the case of the axial planes, the integral can be solved

$$H_z^a = \frac{J_S h_i \cos \vartheta}{8 \mu_0} \left\{ \frac{\sqrt{h_i^2 + q^2}}{h_i^2} - \frac{h_i^2 + q^2 + qR}{h_i^2 \sqrt{h_i^2 + (q+R)^2}} \right. \\ \left. + \frac{3}{4q\sqrt{2}} \left[ 2u_- \tan^{-1}(\sqrt{2}u_-) - 2u_- \tan^{-1}\left(\frac{u_-}{v}(c-R)\right) \right] \right. \\ \left. - \ln \frac{1 - \sqrt{2}u_+}{1 + \sqrt{2}u_+} + \ln \frac{v - u_+(c+R)}{v + u_+(c+R)} \right\} \quad (4)$$

with

$$c^2 = h_i^2 + R^2 + q^2, \quad (5a)$$

$$u_{\pm} = \sqrt{q/(c \pm q)}, \quad (5b)$$

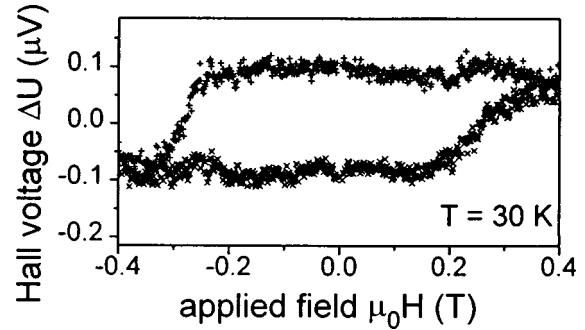


FIG. 2. Measured hysteresis curve of a particle array (cf. Fig. 1) with the applied field parallel to the particles' EMD.

$$v = \sqrt{\frac{1}{2}(c^2 + R^2) + qR}. \quad (5c)$$

Here,  $q$  is the radial distance between the particle's symmetry axis and the point in the Hall cross under consideration and  $\varphi_q$  the corresponding azimuth angle. For the radial plane one finds

$$H_z^r = - \frac{J_S R \cos(\varphi - \varphi_q) \sin \vartheta}{2 \pi \mu_0} \\ \times \int_0^\pi \cos \varphi' d\varphi' \left[ \frac{1}{\sqrt{h_i^2 + q^2 + R^2 - 2qR \cos \varphi'}} \right] \Bigg|_{h_i = z_d}^{z_d + h} \quad (6)$$

with  $\varphi$  being the azimuth angles of the particles' magnetization. The remaining integral was solved numerically. The distances needed for the calculations are taken from AFM and MFM images. Note that, for the dimensions of interest here, the calculated stray fields differ by at most 5% compared to values for a rod of height  $h$  but with square planes of the same area instead of circular planes.

The compensated Hall voltage measured for an array of  $29 \times 21$  particles at a temperature  $T = 30 \text{ K}$  is presented in Fig. 2, showing parts of field sweeps (sweep rate  $20 \text{ mT/min}$ ) from  $\mu_0 H = 1.5 \text{ T}$  to  $-1.5 \text{ T}$  and back to  $1.5 \text{ T}$ . The field is applied parallel to the particles' EMD and hence the switching behavior of the particles' magnetization is observed. The roughly rectangular shape of the hysteresis curve indicates that the particle magnetization stays parallel to the EMD until individual particles reverse their orientation within a relatively small range  $\Delta H_{sw}$  around the mean particle switching field  $H_{sw}$  (for applied field parallel to the EMD,  $H_{sw}$  corresponds to the coercive field  $H_c$ ). The values of  $H_{sw}$  and  $\Delta H_{sw}$  measured for different temperatures are presented in Table I.

Figure 3 shows magnetization curves measured at  $60 \text{ K}$  and for the applied field perpendicular to the easy direction. Prior to this measurement, the sample was magnetized parallel to the particles' EMD in a field of  $1.5 \text{ T}$  and hence the particle magnetization was aligned. Therefore the absolute value of the initially measured Hall response at zero field corresponds to the voltage found for EMD parallel to the field direction. For increasing field the magnetization rotates toward the field direction and is aligned parallel to the applied field for field values larger than the (shape) anisotropy field  $\mu_0 H_A = 2 \mu_0 K_S / J_S \approx 0.7 \text{ T}$ . The field was swept to  $1.5 \text{ T}$

TABLE I. Derived properties of the magnetic particle array shown in Fig. 1 for different temperatures.  $\lambda_{ex}^{cal}$  can only be related to the exchange length  $\lambda_{ex}$  at “zero” temperature.

T [K]	10	30	60	100	
$\mu_0 H_{sw}$ [T]	0.28	0.26	0.24	0.21	$\pm 0.02$
$\mu_0 \Delta H_{sw}$ [T]	0.04	0.09	0.08	0.08	$\pm 0.02$
$m$ [ $10^{-15}$ J/T]	7.9	8.2	7.6	7.5	$\pm 1.0$
$K_S$ [ $\text{MJm}^{-3}$ ]	0.62	0.61	0.61	0.58	$\pm 0.04$
$R$ [nm]	5.0	5.05	4.9	4.85	$\pm 0.3$
$\lambda_{ex}^{cal}$ [nm]	2.5	2.4	2.3	2.2	$\pm 0.4$

followed by sweeps to  $-1.5$  T and back to  $1.5$  T. However, no Hall response was measured for the latter field sweeps. If the field decreases from a value much greater than  $H_A$  to a value less than  $H_A$  the individual magnetizations rotate toward the EMD in a plane given by the EMD and the field. For a field applied exactly perpendicular to the EMD, however, neither of the two easy orientations is preferred and the particles' magnetizations are distributed symmetrically with respect to the field. The symmetry of this distribution is supported by thermally activated switching at fields below but close to  $H_A$  (see below). At zero field, the particles' magnetizations are aligned parallel to the EMD but both orientations are equally probable and hence no net magnetization is measured. The symmetry can be broken by a small misalignment of the field from the perpendicular direction (inset in Fig. 3, angle between EMD and field:  $89.3^\circ$ ). Thus all magnetizations are aligned parallel and their orientation depends on the field polarity.

The field dependence of the Hall response can be calculated using the stray field calculation discussed above. By fitting such curves to the data, a mean value of  $K_S$  and the total magnetic moment  $m$  of all particles can be obtained if all individual magnetizations rotate in the same direction. The results for  $m = n\pi R^2 h \mu_0^{-1} J_S$  are used to estimate the

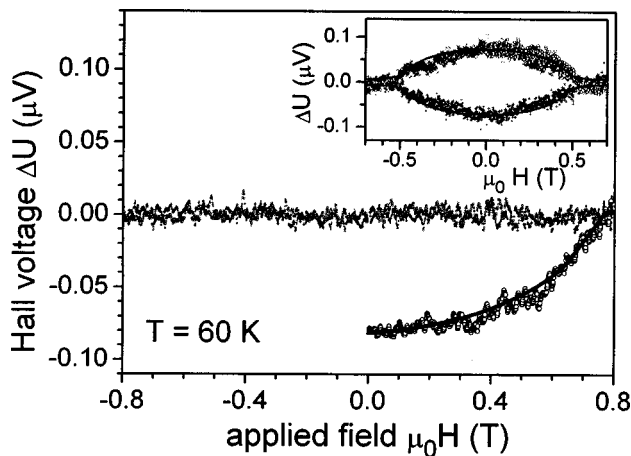


FIG. 3. Magnetization curves (markers) measured for applied field perpendicular to the particles' EMD. The lower branch marks the initial curve obtained after magnetizing the sample parallel to the particles' EMD in a field of  $1.5$  T. The line presents the best fit. For comparison, the inset shows a magnetization curve measured for a field orientation differing slightly from the exact perpendicular orientation.

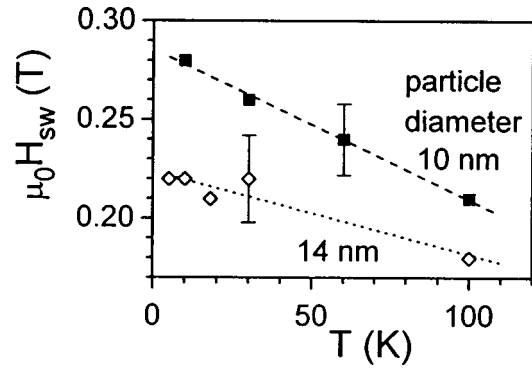


FIG. 4. Switching fields  $H_{sw}$  vs temperature for the array of particles with magnetic core diameter  $10$  nm ( $\square$ ). The line is the proposed  $H_{sw}(T)$  model. Results ( $\diamond$ ) obtained from an array with  $14$  nm particle diameters (from Ref. 5).

radius  $R$  of the particles' magnetic iron core ( $n$ =number of particles). Results of the fits are shown in Fig. 3 (lines) and the values derived at different temperatures are presented in Table I. The good agreement between measured and calculated Hall voltages indicates that the particles' magnetization behavior for perpendicular field orientation can be explained by uniform rotation as initially assumed. Note that the values for  $K_S$  are somewhat lower than those calculated for elongated cylinders ( $\approx 0.90$   $\text{MJm}^{-3}$ ). The determined  $K_S$  are mean values only, and grain boundaries dividing some of the magnetic particles into several grains along their long axis may cause such a reduction. As expected from Eq. (2),  $K_S$  is found to be almost temperature independent.

Assuming magnetization reversal by uniform rotation results<sup>10</sup> in a switching field  $\mu_0 H_{sw} = 2K_S/J_S \approx 0.7$  T which exceeds the measured values by a factor of three and shows only a weak temperature dependence below  $100$  K. This clearly indicates that magnetization reversal involves a non-uniform mode which is likely to be curling for the particle dimensions under consideration.<sup>9</sup> The nucleation field (which equals the switching field) of an infinite cylinder of radius  $R$  calculated for curling mode is given by<sup>8</sup>

$$\mu_0 H_{sw} = 0.54 J_S (\lambda_{ex}/R)^2, \quad (7)$$

where  $\lambda_{ex} = (\mu_0 A)^{1/2}/J_S$  is the exchange length and  $A$  the exchange constant. Values calculated using Eq. (7) are included as  $\lambda_{ex}^{cal}$  in Table I. As will be shown, however, only the “zero” temperature values can be interpreted within the framework of curling. By extrapolation,  $\lambda_{ex} = 2.6$  nm and  $A = 26$   $\text{pJm}^{-1}$  are estimated in agreement with values given elsewhere.<sup>5,13</sup>

The influence of temperature on the magnetization reversal is twofold: (i) via the material properties, and (ii) via thermal fluctuations. The material parameters of interest ( $J_S$ ,  $A$ ,  $K_S$ ) are known<sup>9</sup> to vary only slightly for temperatures below  $100$  K (cf. Table I), suggesting that the large change of  $H_{sw}$  shown in Fig. 4 must be explained by thermal fluctuations. The influence of thermal fluctuations on magnetization reversal was first discussed by Néel<sup>14</sup> and further analyzed by Brown.<sup>15</sup> The two stable magnetization states (moment “up” or “down”) are separated by an energy barrier which decreases with increasing applied field. For a sufficiently large field, the energy barrier can be overcome by

thermal fluctuations and the magnetization reverses. In addition, the smaller the particle volume the smaller the energy barrier, an effect leading ultimately to superparamagnetism.<sup>15</sup> However, an analysis<sup>2</sup> of the temperature dependence of  $H_{sw}(T)$  reveals that  $H_{sw}$  decreases far too rapidly with increasing temperature, using our experimental values of  $K_S$ . Again, this indicates that the magnetization reversal in our particles takes place by a nonuniform mode, in contrast to the nearly spheric particles considered in Ref. 2. In an elongated particle, reversal may take place inhomogeneously along the long axis via a complex path in configuration space which does not involve a single energy barrier.<sup>16</sup>

To interpret the temperature dependence of  $H_{sw}$  for small particles, a phenomenological model is adapted from hard magnetic materials.<sup>17</sup> One assumes a nucleus of reversed magnetization of activation volume,  $v_A$ , separated from the remainder of the particle by a domain wall. For small particles,  $v_A = \pi R^2 l_A$ , where  $l_A$  is a fraction of the particle length. The nucleus and its corresponding domain wall is successfully formed if the gain of magnetostatic energy inside  $v_A$  and the thermal activation equal the wall energy. Thus

$$H_{sw} = \frac{\alpha \gamma}{J_S l_A} - \frac{25 k_B T}{v_A J_S}. \quad (8)$$

The prefactor  $\alpha$  accounts for the number of walls involved in the formation of the nucleus as well as for particle inhomogeneities. For small particles, we assume  $\gamma = 2\sqrt{AK_1}$  independent of the particle dimensions<sup>12,18</sup> (and hence  $K_S$ ) although the actual wall configuration might not be known. At low temperatures,  $v_A$  can be assumed to be temperature independent<sup>17</sup> since it is related to  $\sqrt{A/K_1}$ . Note that Eq. (8) is independent of the actual nucleation mode.

A fit of the dependence  $H_{sw}(T)$  yields  $v_A = 270 \text{ nm}^3$  (see Fig. 4). The experimental values of  $H_{sw}$  are in excellent

agreement with the linear temperature dependence predicted by Eq. (8). Additionally, Eq. (8) predicts that this temperature dependence of  $H_{sw}$  is strongly influenced by the particles' radius  $R$  but not by their length. The former effect is demonstrated in Fig. 4: the switching fields of particles of 14 nm diameter<sup>5</sup> are less influenced by thermal fluctuations [a rough estimation yields  $v_A = 480 \text{ nm}^3$  supporting  $v_A \propto R^2$  as inferred from Eq. (8)] than their smaller counterpart. The value  $\alpha \approx 0.8$  may indicate a magnetization reversal nucleating at one end of a particle, a behavior also found by simulation calculations.<sup>19</sup> Equation (8) as well as the experimental results listed above are in agreement with investigations on magnetic viscosity<sup>18-20</sup> for similar particle dimensions.

In conclusion, the magnetic properties of nanometer-scale iron particles of regular shape and alignment (magnetic moment, mean shape anisotropy, switching field, and distribution) have been investigated by measuring magnetization curves for fields applied in different directions. The measured switching fields indicate that magnetization reversal occurs by curling at "zero" temperature, and an exchange length,  $\lambda_{ex} = 2.6 \text{ nm}$ , is estimated. At higher temperatures up to 100 K, thermal activation in a nucleation volume of  $(6.5 \text{ nm})^3$  also contributes to the reversal. This volume is much smaller than that of the physical particle which may explain why the magnetization reversal in the present case cannot be described in terms of excitations over a single energy barrier.<sup>2</sup> A phenomenological model was introduced which accounts for the linear dependence of the switching field on temperature and strong influence of the particles' diameter which are observed experimentally.

This work was supported by NSF Grant Nos. DMR 95-27553 and DMR 95-10518 and AFOSR Grant No. F49620-96-0018. S.W. is supported by the Alexander von Humboldt Foundation, Germany.

<sup>1</sup>W. Wernsdorfer *et al.*, Phys. Rev. Lett. **77**, 1873 (1996).

<sup>2</sup>W. Wernsdorfer *et al.*, Phys. Rev. Lett. **78**, 1791 (1997).

<sup>3</sup>A. D. Kent, T. M. Shaw, S. von Molnár, and D. D. Awschalom, Science **262**, 1249 (1993).

<sup>4</sup>A. D. Kent, S. von Molnár, S. Gider, and D. D. Awschalom, J. Appl. Phys. **76**, 6656 (1994).

<sup>5</sup>S. Wirth *et al.*, IEEE Trans. Magn. (to be published).

<sup>6</sup>S. Gider *et al.*, Appl. Phys. Lett. **69**, 3269 (1996).

<sup>7</sup>W. F. Brown, Jr., Phys. Rev. **105**, 1479 (1957).

<sup>8</sup>E. H. Frei, S. Shtrikman, and D. Treves, Phys. Rev. **106**, 446 (1957).

<sup>9</sup>A. Aharoni, *Introduction to the Theory of Ferromagnetism* (Oxford University Press, New York, 1996).

<sup>10</sup>E. C. Stoner and E. P. Wohlfarth, Philos. Trans. R. Soc. London, Ser. A **240**, 599 (1948).

<sup>11</sup>G. Asti *et al.*, J. Appl. Phys. **76**, 6268 (1994).

<sup>12</sup>E. Kneller, *Ferromagnetism* (Springer, Berlin, 1962), p. 293.

<sup>13</sup>L. R. Bickford, Phys. Rev. **78**, 449 (1950).

<sup>14</sup>L. Néel, Ann. Geophys. (C.N.R.S.) **5**, 99 (1949).

<sup>15</sup>W. F. Brown, Jr., Phys. Rev. **130**, 1677 (1963).

<sup>16</sup>M. Lederman, S. Schultz, and M. Ozaki, Phys. Rev. Lett. **73**, 1986 (1994).

<sup>17</sup>D. Givord, P. Tenaud, and T. Viadieu, IEEE Trans. Magn. **24**, 1921 (1988).

<sup>18</sup>H.-B. Braun, Phys. Rev. B **50**, 16 501 (1994).

<sup>19</sup>E. D. Boerner and H. N. Bertram, IEEE Trans. Magn. **33**, 3052 (1997).

<sup>20</sup>Feiyue Li, R. M. Metzger, and W. D. Doyle, IEEE Trans. Magn. **33**, 3715 (1997).